RSC Advances

PAPER

View Article Online
View Journal | View Issue

Cite this: *RSC Adv.*, 2025, **15**, 7728

Cobalt–nickel composite nano-grass as an excellent electrode for urea oxidation†

Norah Alwadai,[a] Manar Alshatwi[a] and Enas Taha Sayed *[ab]

Urea-contaminated wastewater requires extensive energy for proper treatment before safe discharge to the surroundings. Direct urea fuel cells (DUFCs) could be utilized efficiently to treat urea-polluted water and generate electricity. The precious/expensive catalyst utilized at the electrodes is one of the main significant challenges to DUFC commercialization. In this study, a non-precious standalone electrode cobalt–nickel composites directly formed using a facile hydrothermal method on a highly porous conductive nickel foam (NF) surface. The developed electrode has an excellent nano-grass morphology and demonstrates outstanding activity towards urea electro-oxidation. Using a 0.33 M urea, the current density @ 0.5 V (*vs.* Ag/AgCl) in the case of the cobalt–nickel composite with the nano-grass electrode (Co/NF) is significantly higher than that obtained using the bare NF electrode. At the same conditions, the Co/NF electrode is successfully operated for a long term (24 h) with a slight degradation in the performance, with no effect on the surface morphology. The steady-state current generated after 24 hours of cell operation is twenty times that obtained using the bare NF. The perfect performance of the modified electrode is related to the synergetic effect between Ni and Co, excellent nano-grass morphology, and ease of charge transfer. The prepared materials on the surface of the NF have a high electrochemically active surface area of 44 cm^2 that is significantly higher than that of bare NF.

Received 6th November 2024
Accepted 26th February 2025

DOI: 10.1039/d4ra07911f

rsc.li/rsc-advances

1. Introduction

The convergence of environmental and energy issues creates a complex dilemma that is critical to our planet's sustainability.[1] The environmental impact of energy is a multifaceted issue, involving not only the direct consequences of energy production and consumption but also the broader effects on ecosystems and human health.[2] For instance, the extraction and burning of fossil fuels result in emissions that contribute to air pollution and climate change, while posing risks to water quality and biodiversity. The current global energy crisis exacerbates these concerns, emphasizing the critical need for a shift to cleaner and more sustainable energy sources. One of the best ways to achieve net-zero emissions is the usage of safe, inexpensive, and low-carbon large-scale energy options in place of fossil fuels.[3] The energy crisis has also highlighted the opportunity to accelerate the implementation of renewable energy sources like wind, biomass, solar, and geothermal, energies.[4] These energy resources, which were formerly considered futuristic, are now widely regarded as realistic solutions to our energy demands. Biomass is among the different renewable energy sources that is globally abundant and is produced on a daily basis in the form of municipal wastes and wastewater.

Urea is typically found in agricultural runoff and urban wastewater since it is naturally produced by human metabolism and is used as an inexpensive nitrogen fertilizer.[5,6] Improper management of urea-polluted wastewater can result in serious environmental issues such as eutrophication, water pollution and damage to aquatic ecosystems.[7] Urea treatment and management strategies are crucial to minimizing the environmental impact of urea and ensuring the sustainability of our water resources.[8]

Fuel cells (FCs) are interesting new devices that could be implemented for direct electricity generation from various fuels with high efficiency at minimal or no environmental impact. FCs are available in different capacities and can be operated at various conditions, from room to very high operating temperatures.[9,10] An innovative and sustainable energy generation technology is urea fuel cell.[11] Urea, which is widely found in human and animal waste, as well as in industrial effluents, can be effectively transformed into electricity *via* fuel cells.[12] Urea fuel cells are an innovative branch of green technology that uses the chemical energy of urea to generate electricity.[12] The mechanism of urea fuel cells involves electrochemical reactions in which urea is degraded into nitrogen, water, and carbon dioxide while simultaneously producing electricity.

Notwithstanding the possible advantages, there are obstacles to be addressed, such as the synthesis of effective catalysts

[a]*Department of Physics, College of Science, Princess Nourah bint Abdulrahman University, P.O. Box 84428, Riyadh 11671, Saudi Arabia. E-mail: e.kasem@mu.edu.eg*
[b]*Sustainable Energy & Power Systems Research Centre, RISE, University of Sharjah, P.O. Box 27272, Sharjah, United Arab Emirates*

† Electronic supplementary information (ESI) available. See DOI: https://doi.org/10.1039/d4ra07911f

that can boost the urea oxidation process without using precious metals like platinum.[13] Developments in this field may result in more accessible and sustainable energy options, promoting the development of greener technology. Developing efficient and cost-effective catalysts for the urea oxidation reaction (UOR) will make urea fuel cells more practical and efficient, making them a promising alternative sustainable energy source.[14] Nickel demonstrated a considerable activity towards the urea oxidation.[15–17] Nickel's activity is boosted by increasing its surface area using high surface area supports such as graphene,[18,19] carbon nanofibers,[20,21] and carbon nanotubes.[22] Alloying nickel with other transition metals also improved the electrochemical activity of nickel towards urea electro-oxidation.[23] Alloying nickel with a co-catalyst such as manganese,[24] MnO_2,[25] copper,[26] and cobalt[27] resulted in improving the activity of nickel towards urea oxidation. Nickel ferrocyanide prepared on the surface of nickel foam demonstrated high activity toward urea oxidation.[28]

Cobalt is one of the transition metals that is commonly used to enhance the activity of nickel towards the oxidation of urea and other simple alcohols (methanol and ethanol). Doping nickel with cobalt improves its catalytic activity up to a certain limit, which can be attributed to several factors: cobalt acts as a co-catalyst by providing OH groups, thereby reducing CO poisoning;[29,30] it facilitates fuel molecule adsorption *via* its partially vacant d-orbitals and serves as a CO anti-poisoning agent;[31] it modifies structural and electronic properties;[32] and it enhances the oxidation state of Ni, thereby improving electron transfer.[33] Additionally, alloying nickel with cobalt has been reported to lower the onset potential for fuel oxidation, potentially due to the formation of CoOOH, which has a lower redox potential than NiOOH.[34] An increase in Co content in NiCo alloys generally lowers the onset potential,[35] attributed to the formation of CoOOH at a lower potential than Ni. Notably, the lowest reported onset potential for methanol oxidation in alkaline media using $Ni_{0.5}Co_{0.5}$/CNF is 0.11 V (*vs.* Ag/AgCl),[36] while for ethanol oxidation, $Ni_{0.1}Co_{0.9}$/CNF achieved −50 mV (*vs.* Ag/AgCl).[37] The doping of $Co(OH)_2$ with nickel nanoparticles significantly increased UOR activity with a low onset potential of 1.15 V *vs.* RHE compared to nickel nanoparticles or $Co(OH)_2$. The authors confirmed that nickel nanoparticles serve as the active sites for UOR, while $Co(OH)_2$ acts as a support, providing a high surface area and a conductive pathway for electrons. They also observed that increasing the nickel content led to a higher onset potential.[38] Liu *et al.*[39] prepared Ni_xCo_{3-x}-O with a nanowire morphology on the surface of carbon cloth (Ni_xCo_{3-x}-O/CC). Among the different nickel-to-cobalt ratios, $Ni_{1.5}Co_{1.5}$-O/CC exhibited the best UOR activity using 0.33 M urea in 1 M KOH. NiCo BMHs "nickel–cobalt bimetallic hydroxides" with enriched nano-holes having a high surface area demonstrated a high UOR activity that related to the high surface area, synergetic effect between the Ni^{2+} and Co^{2+}/Co^{3+}, and high surface defects.[40] Ismail *et al.*[41] prepared Co_3O_4 with different morphologies, *i.e.*, nanoparticles, nanowires, and nanocubes on the surface of nickel foam. The Co_3O_4 with nanocubes morphology demonstrated the best UOR activity that related to its higher surface area and lower agglomeration. The Co_3O_4 nanocubes demonstrated high stability with low onset potential of 197 mV *vs.* Hg/HgO and CoOOH is considered the active site for UOR.

Although extensive work relies on the alloying of the nickel with co-catalyst and/or using high surface area support, commercial non-precious catalysts are still unavailable. Moreover, these catalysts are usually prepared in a nanoparticle form that should be deposited on a highly conductive porous substrate (such as NF or carbon cloth) to form the anode electrode. During the deposition of these nano-catalysts, a part of the catalyst is lost through the pores of the support while blocking part of the substrate's pores (negatively influencing the mass transfer characteristics of the electrodes). Furthermore, a Nafion or Teflon binder (with no electrical conductivity) is usually used to bind the catalyst with each other and with the substrate, which eventually decreases the conductivity (electrical) of the prepared electrode.

Herein, using a hydrothermal approach, a standalone anode is prepared by the direct growth of cobalt–nickel composite nano-grass on the surface of NF (Co/NF). The surface morphology, elemental analysis, and crystalline structure of the electrodes are investigated and compared with the bare NF. The catalytic activity of the prepared electrode towards urea oxidation is tested and compared with that of the bare NF. The obtained results are discussed based on the surface morphology, charge and mass transfer, and the electrochemical active sites of the modified and the bare electrodes.

2. Experimental work

2.1 Materials and methods

Cobalt nitrate ($Co(NO_3)_2 \cdot 6H_2O$), KOH, urea, hydrofluoric acid (HF), ethanol, acetone, and other chemicals are all obtained from Sigma Aldrich (Merck). Ultra-pure deionized water (DI) of 20 MΩ was used for all the experiments. A 2×5 cm^2 nickel foam (NF) of 2 mm thickness is cleaned in 0.1 M HCl for 15 min (ultrasound path), in DI water for 15 min (ultrasound path), in acetone for 15 min (ultrasound path), and finally in DI water again for 15 min (ultrasound path). The cleaned foams are then dried in an oven overnight at 60 °C.

2.2 Preparing of the cobalt–nickel composite nano-grass over the nickel foam

The cleaned Ni foam was inserted into an autoclave (Teflon lined stainless steel) containing a solution. The solution is composed of cobalt nitrate and urea (1 g each) in a 50 ml DI water containing a 0.2 ml of HF (48%). The autoclave after tightly closed is inserted in an oven that held at 120 °C for 6 h.[42,43] After leaving the oven to decrease to the room temperature gradually, the autoclave is removed from the oven. The sample is removed and carefully cleaned with water to remove the surface agglomerates, and then, it is inserted into a beaker containing water (24 h). Then the sample is removed and dried under vacuum at 60 °C for 12 h.

2.3 Characterization of $Co(OH)_2$ nano-grass

The electrodes were investigated using SEM "scanning electron microscope" to see the surface morphology. The elemental

analysis was also detected using an EDS analyzer attached to the SEM device. The crystalline structure was investigated by XRD "TESCAN VEGA3, Bruker D8", while the surface analysis is determined *via* XPS "Thermo Scientific, UK". TEM "Transmission electron microscopy", and HRTEM "High Resolution Transmission electron microscopy" images were taken using JEOL, JEM-2100Plus.

2.4 Electrochemical characterization

The electrochemical activity of NF and the NF after growing the cobalt–nickel composite on its surface (Co/NF) is investigated in 1 M KOH solution with and without different concentrations of urea (0 M to 0.5 M) in a three-electrode cell structure (counter electrode (Pt sheet of 1 cm^2), reference electrode (Ag/AgCl), and working electrode (NF or Co/NF fixed in a Pt holder)). Both the NF and the Co/NF have an area of 1 cm^2 (1 cm × 1 cm). Cyclic voltammetry was carried out at 0.05 V s^{-1} for 100 cycles in urea-free KOH solution @ room temperature to activate the electrodes (−0.2 V to 0.8 V *vs.* Ag/AgCl). Then, the electrochemical oxidation activity of the samples (NF and Co/NF) are tested at 0.02 V s^{-1} between 0 and 0.6 V in KOH (1 M) containing different urea (0, 0.1, 0.33, and 0.5 M). EIS "electrochemical impedance spectroscopy" is carried out for the two electrodes in 0.33 M urea @ 0.5 V (*vs.* Ag/AgCl) between 100 kHz and 100 mHz. The stability of the bare and the prepared electrodes is tested through chronoamperometry measurements @ 0.5 V (*vs.* Ag/AgCl) for long-term operation using 0.33 M urea.[44,45] All voltages mentioned in the current work are *vs.* Ag/AgCl. The ECSA "electrochemical active surface area" for the NF and Co/NF electrodes is determined by performing cyclic voltammetry in a non-Faradic region in urea-free 1 M KOH.[46,47]

3. Results and discussions

3.1 Characterization of NF and Co/NF

The surface morphology of the bare NF is displayed in Fig. 1A and B at low and high magnifications, respectively. As clear from Fig. 1A, the NF has an interconnected network of highly porous structure, and the surface of the metal parts is smooth as can be seen at high resolution (Fig. 1B). The Co/NF has an excellent nano-grass morphology as seen in Fig. 1C. These nano-grass structures are a few micrometres in length, as indicated by the blue line in Fig. 1D. The nano-grass morphology is also evident in the TEM images (Fig. 1F), where the structures exhibit a needle-like shape, with a wide base diameter of around 100 nm that tapers to less than a few nanometers at the tip. EDS analysis confirms the presence of cobalt, nickel, oxygen, and gold (due to gold plating), as shown in the inset of Fig. 1C. The XRD of the bare NF and modified Co/NF is shown in Fig. 1E. The NF demonstrated three sharp peaks that are related to Ni (111), (200), and (220).[48,49] The XRD pattern of Co/NF-1 exhibited the sharp peaks of the base Ni foam, with no clear peaks corresponding to $Co(OH)_2$. This may be attributed to the high intensity of the crystallographic planes of Ni foam. To gain further insight, the grown dendrites on the surface of the NF was carefully detached from the Ni foam *via* ultra-sonication and analyzed by XRD, Co/NF-2. The XRD analysis of the Co/NF-2 revealed distinct peaks corresponding to the crystallographic planes (001), (100), (102), and (110) of $Co(OH)_2$ (ICDD: 00-030-0443).[50–52] Furthermore, the presence of $Co(OH)_2$ was supported by Raman spectroscopy and XPS analysis, providing additional structural confirmation. The HRTEM image (Fig. 1G) revealed a lattice fringe with a spacing of 0.28 nm, which corresponds to the interplanar distance of the (100) crystallographic planes of $Co(OH)_2$. The diffraction dots

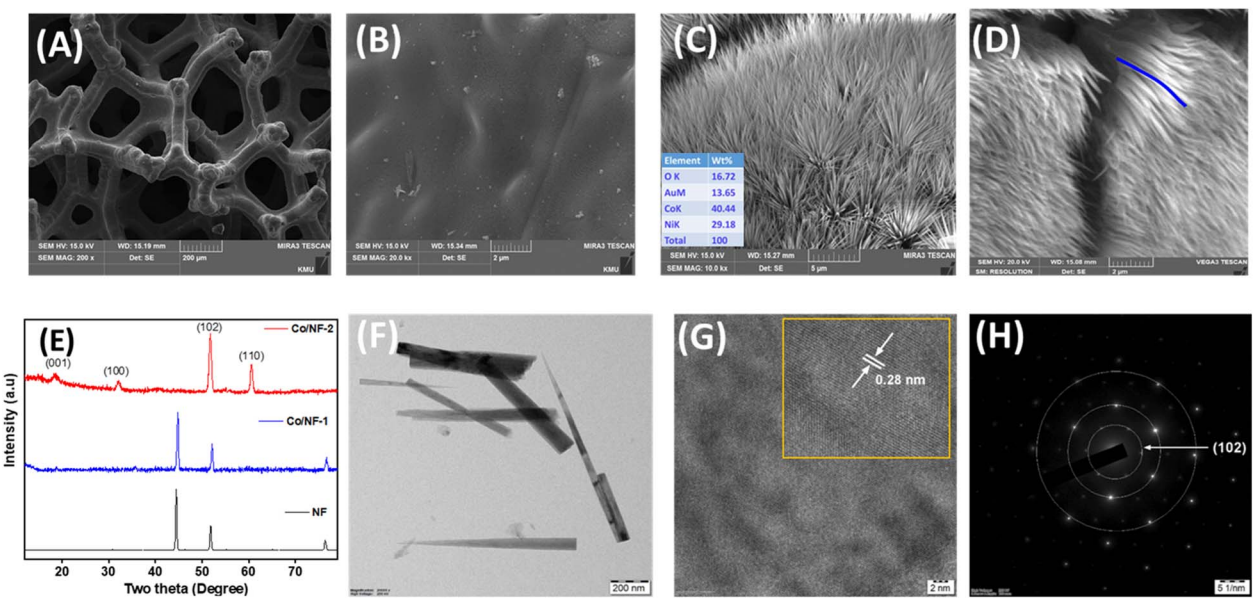

Fig. 1 (A) low-resolution image of NF, (B) high-resolution image of NF, (C and D) high-resolution image of the Co/NF (inset in (C) shows the elemental analysis, while the blue line in (D) shows the length of the nano-grass), (E) XRD of NF, Co/NF-1, and Co/NF-2, (F) TEM images of the Co/NF, (G) HRTEM of the Co/NF, and (H) SAED of Co/NF.

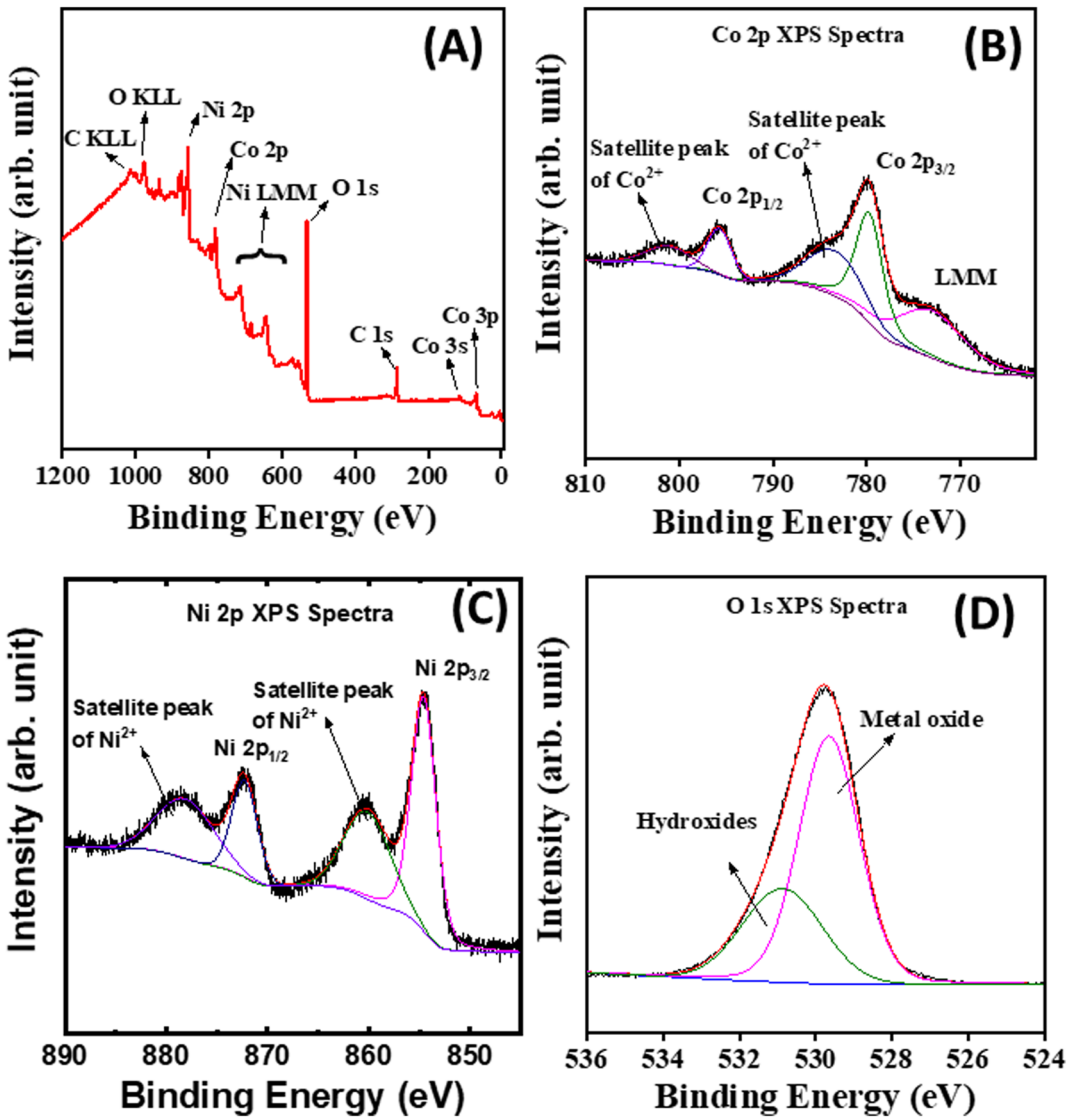

Fig. 2 (A) XPS survey of the Co/NF, (B) deconvolution of the Co 2p XPS spectra, (C) deconvolution of the Ni 2p XPS spectra, and (D) deconvolution of the O 1s XPS spectra.

looked in the SAED of the prepared material established its high crystallinity. The crystallographic plane (102) of $Co(OH)_2$ is indexed in the SAED pattern as provided in Fig. 1H.

The XPS survey spectrum, Fig. 2A, clearly shows Co, Ni, and O for the Co/NF electrode. The presence of C appeared from the adventitious carbon from the XPS instrument. The high-resolution XPS spectrum of Co, Fig. 2B, can be de-convoluted into four peaks (because of the spin-orbital coupling). The peaks at ~779.8 and ~795.7 eV attribute to Co $2p_{3/2}$ and Co $2p_{1/2}$, respectively, and the peaks at ~784.7 and ~801.3 eV of Co are the satellite peaks. The Co 2p spectra were fitted by a sufficient number of Voight-type functions which optimized without constraints, considering two spin–orbit coupling and two satellite peaks. As revealed in this figure, the binding energies at around ~779.8 and ~795.7 eV indicate the existence of Co^{2+}. Also, the weak satellite peaks are characteristics of Co^{2+} state. The deconvoluted Ni 2p XPS spectrum, Fig. 2C, revealed two major peaks at 854.7 and 872.4 eV, corresponding to $2p_{3/2}$ and

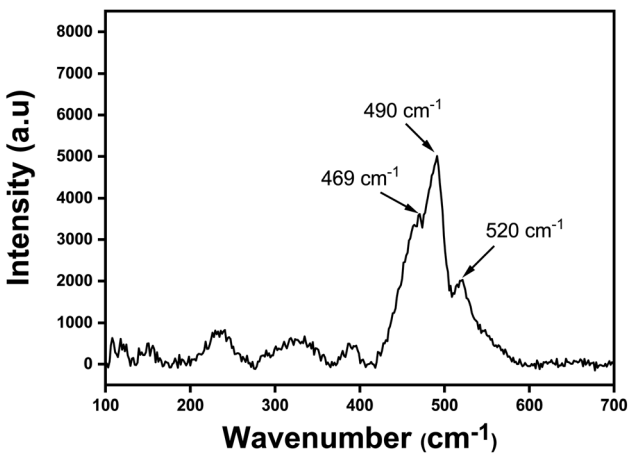

Fig. 3 Raman spectra of Co/NF sample.

$2p_{1/2}$ of Ni^{2+} present in the material. In addition to these, two satellite peaks are also observed at 860.4 and 878.5 eV. The appearance of these peaks confirms the presence of Ni^{2+} arising from the surface oxidized NiO.[53,54] The deconvoluted O 1s XPS spectrum, Fig. 2D, displayed two major peaks at 529.7 and 530.9 eV which are associated with the oxygen in the metal–oxygen (M-O) bond and hydroxide (OH^-), respectively, in the material.

Raman was carried out to detect the surface analysis of the modified sample (Co/NF) as can be seen in Fig. 3. As seen in the figure, the presence of $Co(OH)_2$ is confirmed by the existence of a RAMAN peak at 520 cm^{-1}, which is due to the Co–O (A_g) symmetric stretching mode present in $Co(OH)_2$ in addition to the other peak observed at 469 cm^{-1} due to O–Co–O bending mode of $Co(OH)_2$.[55] The existence of $Ni(OH)_2$ in the Co/NF sample is also confirmed by the appearance of the strong characteristic peak at 490 cm^{-1} for Ni–O vibration.[56]

3.2 Electrochemical measurements

The electrochemical activities of NF and Co/NF electrodes were tested in alkaline media (1 M KOH) with and without urea. A redox peak in a urea-free solution (0 M urea) is clearly observed in both electrodes—bare NF and Co/NF—around 0.35 V *vs.* Ag/AgCl. However, the Co/NF electrode exhibited stronger redox peaks in urea-free KOH than bare NF. Adding urea (0.1 M and 0.33 M) to the 1 M KOH solution increased the current in the forward scan compared to the urea-free solution for both electrodes. This increase in current began (onset potential for UOR) around 0.35 V *vs.* Ag/AgCl, confirming that the active site for urea oxidation originates from Ni ($NiOOH/Ni(OH)_2$).[57] In the case of NF, NiOOH forms on the surface and acts as the active site. For the Co/NF electrode, NiOOH originates from the nickel in the base NF, and the nickel presents in the cobalt–nickel composite nano-grass, as confirmed by XRD (Fig. 1E), XPS (Fig. 2), and Raman spectroscopy (Fig. 3). Therefore, $NiOOH/Ni(OH)_2$ serves as the active site for UOR, while cobalt acts as a co-catalyst, enhancing the catalytic activity as described above.

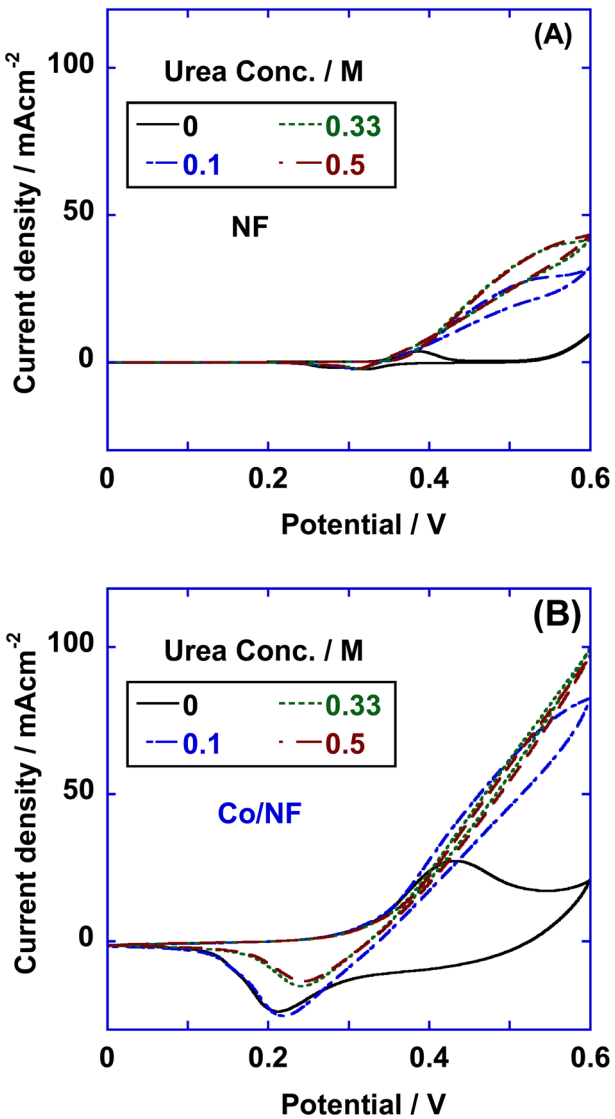

Fig. 4 CV of the bare NF (A) and Co/NF (B) using different urea concentrations @ 20 mV s^{-1}. Voltages are *vs.* Ag/AgCl, and the electrolyte used is 1 M KOH.

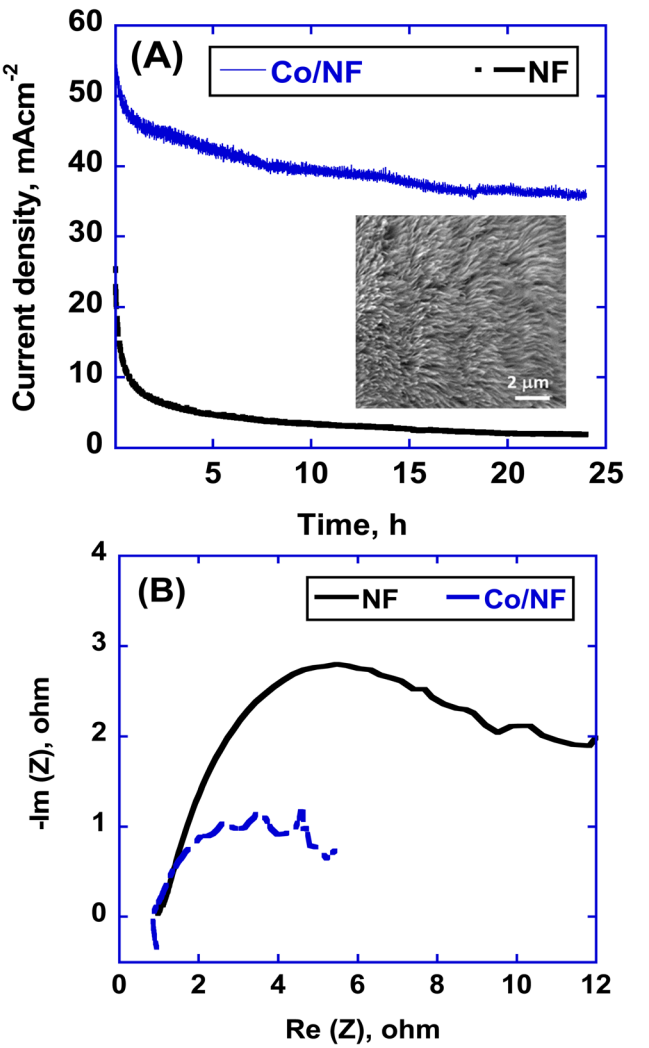

Fig. 5 (A) Chronoamperometry measurement @ 0.5 V using NF and Co/NF, and (B) EIS of bare NF and Co/NF using 0.33 M and 0.5 V. Voltages are *vs.* Ag/AgCl, and the electrolyte used is 1 M KOH.

As shown in Fig. 4, during the forward scan, the current increases as the urea concentration rises to 0.33 M, then stabilizes in both cases—bare NF (Fig. 4A) and Co/NF (Fig. 4B). Additionally, Co/NF exhibited a higher current density than bare NF at different urea concentrations. For instance, at 0.5 V (*vs.* Ag/AgCl) with 0.33 M urea, the Co/NF electrode generated 60 mA cm^{-2}, twice the NF's current density (30 mA cm^{-2}).

The high current density in the Co/NF sample could be attributed to: (1) the role of cobalt as a co-catalyst, which enhances UOR activity, and (2) the high surface area of the nano-grass grown on the nickel foam, as observed in the electron microscope images (Fig. 1C and D). These factors increase both the number and the quality of active sites available for urea oxidation, leading to higher current densities compared to bare NF under the same applied voltage and urea concentrations.

The cyclic voltammograms (Fig. 4) describe the instantaneous current generated using the different electrodes at different voltages, which do not show stable current generation. The steady current generation is determined by operating the electrodes, *i.e.*, the bare NF and the Co/NF, at 0.5 V (*vs.* Ag/AgCl) for 24 hours, as shown in Fig. 5A. Co/NF produces an initial current density around 55 mA cm^{-2} that is almost twice that obtained using the bare NF. The current density in both cases slightly decreases with time, and it reaches 36 mA cm^{-2} in the case of the Co/NF, which is almost twenty times that generated using the NF (after 24 h). These results showed the high stability of the Co/NF electrode with a degradation rate of 0.79 mA cm^{-2} h^{-1}, compared with 1.4 mA cm^{-2} h^{-1} in the case of the bare NF. It is worth mentioning that bubble formation on the electrode surface is one of the main reasons for current degradation, as it blocks urea access to the active sites. This effect is more pronounced at high current densities, where increased bubble formation is observed, particularly in the case of the Co/NF electrode. As described above, the high activity of the Co/NF electrode would be related to the role of the cobalt as a co-catalyst and the high surface area of the nano-grass with plenty of active sites compared with the bare NF. To better show the stability of the Co/NF electrode, the SEM images of the electrode at the end of the experiment were tested, as can be seen in the inset of Fig. 5A. It is clear that the electrode still kept perfect nano-grass morphology even after 24 h of current generation. The electrochemical behaviour of the bare and modified electrode is also investigated by performing EIS "Electrochemical Impedance Spectroscopy" measurements at 0.5 V (*vs.* Ag/Ag/Cl) using 0.33 M urea, Fig. 5B. It is clear from the figure the improved charge and mass transfer characteristics of the modified electrode (Co/NF) as can be seen in the intersect with the *X*-

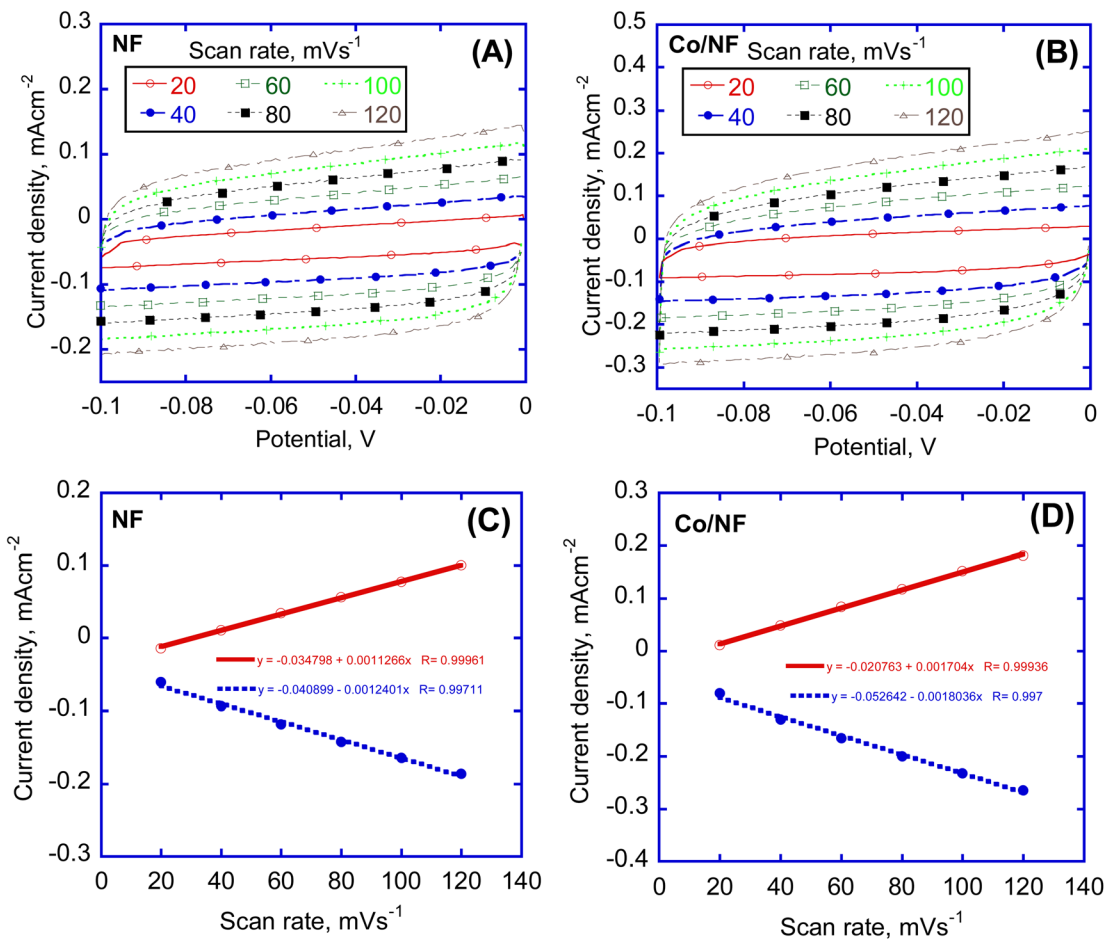

Fig. 6 (A) CVs of the NF and (B) CVs of the Co/NF using different scan rates, (C) the current density @ −0.05 V *vs.* scan rate in case of the NF, and (D) the current density @ −0.05 V *vs.* scan rate in case of the Co/NF, voltages are *vs.* Ag/AgCl, and the electrolyte used is 1 M KOH.

Table 1 Example of some catalysts prepared and tested against urea electro-oxidation *versus* those obtained in this study

Working electrode	Counter electrode	Urea conc. (M)	Scan rate (mV s^{-1})	Onset potential (V *vs.* RHE)	Current density @ 1.5 V (mA cm^{-2})	Ref.
$Ni(OH)_2$ NS/GC	Pt	0.33	50	1.4	35	65
Ni-MOF/GC	—	0.33	10	1.4	~60	66
$Ni(OH)_2$	—	0.33	10	1.5	~20	66
Ni-MOF	Pt foil	1	20	1.4	~25	67
$Ni_{0.8}Co_{0.2}(OH)_2$	Pt wire	0.2	20	1.3	120	68
$Ni(OH)_2$	Pt wire	0.2	20	1.4	60	68
$Ni_{1.5}Co_{1.5}$-O/CC	Graphite rod	0.33	5	1.4	~95	39
Ni–Fe LDH/EG-GC	Pt foil	0.33	—	1.3	~175	72
CoFe LDH/NF	Pt	0.33	1	1.4	~75	69
CoFeCr LDH nanosheets/NF	Pt	0.33	1	1.3	~190	69
$Ni_{12}P_5$/NF	Graphite rod	0.5	5	1.2	~145	70
$NiSe_2$/TiN@$Ni_{12}P_5$/NF	Graphite rod	0.5	5	1.2	~150	70
$NiMoO_4$ NS/NF	Graphite rod	0.5	—	1.3	~150	73
Co/NF	Pt foil	0.33	20	1.4	83	This study

axis and the smaller semi-circuit diameter.[58–60] The high fluctuations at the low frequency in the case of the Co/NF could be connected to the rapid reaction rate that resulted in excessive evolution of the bubbles that are clear in this region and interrupting the mass transfer.

Although the images in Fig. 1 clearly show the significant difference in the surface morphology between the NF and the Co/NF electrodes, it is important to calculate the ECSA "electrochemical active surface area" that directly reflects the electrodes' reaction rate. The ECSA can be calculated using the values of the C_{dl} "electrochemical double layer capacitance" and C_s "specific electrochemical double layer capacitance". C_{dl} is the ratio between the discharge current (i_c) and the scan rate (v) in the non-Faradic region within 100 mV.[61–64] To calculate the C_{dl}, the CV of the NF and Co/NF electrodes are tested in a non-Faradic region −0.1 V to 0 V (*vs.* Ag/AgCl) using 1 M KOH solution, Fig. 6A and B. Then the C_{dl} is calculated as the slope of the current at −0.05 V *vs.* the scan rates, Fig. 6C (in the case of the bare NF) and Fig. 6D (in the case of the Co/NF). The C_{dl} is calculated as the average of the absolute slopes, and it is found to be 1.183 mF in the case of the NF, and 1.77 mF in the case of the Co/NF. Using the C_s of 0.04 mF cm^{-2},[61–64] the ECSA in the case of the NF is found to be 29.6 cm^2 compared with 44.25 cm^2 in the case of Co/NF. Such higher ECSA describes the significantly high activity of the Co/NF electrode (Fig. 4 and 5).

As seen in Table 1, the obtained results in this research are similar to those reported in the literature. In general, they are better than a single catalyst, such as the case of the $Ni(OH)_2$ with different morphologies,[65–68] and they are close to the results of binary catalysts, such as the case of the $Ni_{1.5}Co_{1.5}$-O/CC,[39] and the case of CoFe LDH/NF.[69] However, the current results are lower than those reported using tertiary catalyst combinations, such as the case of the CoFeCr LDH nanosheets/NF,[69] and the case of $NiSe_2$/TiN@$Ni_{12}P_5$/NF.[70] Moreover, the prepared catalyst in this study has the merit of direct growth on the NF (high porous conductive substrate), and the prepared material is used as a standalone electrode with better mass transfer properties as well as durability compared with the cases of preparing the nanoparticle catalyst followed by their deposition on the surface of the substrate. The latter case involves using a binder that is usually polymer-based with low or no electrical conductivity (such as Nafion or Teflon solutions) and thus decreases the electrical conductivity as well as blocking part of the pores of the porous substrate, thereby decreasing the electrical conductivity and the mass transfer property of the electrode.[71]

4. Conclusions

A standalone electrode composed of cobalt–nickel composites with a perfect nano-grass morphology is successfully prepared on the surface of a highly porous conductive nickel foam using a one-step hydrothermal method. The nano-grass electrode demonstrated a higher urea oxidation activity than that of the bare NF. The Co/NF exhibited better charge transfer properties (verified from the CV and the EIS) that could be connected to the role of the cobalt as a co-catalyst and the nano-grass's highly porous texture on the nickel foam's surface. The long-term operation was verified for 24 hours of cell operation. The steady current after 24 hours of cell operation is twenty times that of the bare NF, with a lower degradation rate. The surface morphology of the Co/NF electrode was not affected by the long-term operation. The good electrochemical performance of the prepared electrodes would be related to the role of the cobalt as co-catalyst and the high surface area of the nano-grass morphology that resulted in a higher electrochemical active surface area than that of the bare NF. The prepared electrode with the perfect mass and charge transfer properties is a promising, cheap, durable electrode for urea oxidation.

Data availability

Data related to this research are included in the current version.

Author contributions

Conceptualization: Enas Taha Sayed. Formal analysis: Norah Alwadai, Manar Alshatwi, Enas Taha Sayed. Investigation: Norah Alwadai. Methodology: Manar Alshatwi, Enas Taha Sayed. Project administration: Norah Alwadai. Supervision:

Norah Alwadai, Enas Taha Sayed. Writing – original draft: Norah Alwadai, Manar Alshatwi, Enas Taha Sayed. Writing – review & editing: Norah Alwadai, Manar Alshatwi, Enas Taha Sayed.

Conflicts of interest

There are no conflicts of interest to declare.

Acknowledgements

The authors express their gratitude to Princess Nourah bint Abdulrahman University Researchers Supporting Project number (HCPNU2024R11), Princess Nourah bint Abdulrahman University, Riyadh, Saudi Arabia".

References

1 P. O. Ukaogo, U. Ewuzie and C. V. Onwuka, Environmental pollution: causes, effects, and the remedies, in *Microorganisms for Sustainable Environment and Health*, Elsevier, 2020, pp 419–429.
2 Q. Hassan, P. Viktor, T. J. Al-Musawi, B. M. Ali, S. Algburi, H. M. Alzoubi, A. K. Al-Jiboory, A. Z. Sameen, H. M. Salman and M. Jaszczur, The renewable energy role in the global energy Transformations, *Renew. Energy Focus*, 2024, **48**, 100545.
3 S. K. M. Balgehshiri and B. Zohuri, The Impact of Energy Transition to Net-Zero Emissions on The World Economy and Global Strategies, *J. Econ. Manage. Res.*, 2023, **185**, 2–7, DOI: 10.47363/JESMR/2023(4)185.
4 O. Ostapenko, G. Alina, M. Serikova, L. Popp, T. Kurbatova and Z. Bashu, Towards Overcoming Energy Crisis and Energy Transition Acceleration: Evaluation of Economic and Environmental Perspectives of Renewable Energy Development, in *Circular Economy for Renewable Energy*, Springer, 2023, pp. 109–128.
5 X. Zhuo, W. Jiang, G. Qian, J. Chen, T. Yu, L. Luo, L. Lu, Y. Chen and S. Yin, Ni_3S_2/Ni heterostructure nanobelt arrays as bifunctional catalysts for urea-rich wastewater degradation, *ACS Appl. Mater. Interfaces*, 2021, **13**(30), 35709–35718.
6 J. d. D. M. Ufitikirezi, M. Filip, M. Ghorbani, T. Zoubek, P. Olšan, R. Bumbálek, M. Strob, P. Bartoš, S. N. Umurungi and Y. T. Murindangabo, Agricultural Waste Valorization: Exploring Environmentally Friendly Approaches to Bioenergy Conversion, *Sustainability*, 2024, **16**(9), 3617.
7 D. Weerakoon, B. Bansal, L. P. Padhye, A. Rachmani, L. J. Wright, G. S. Roberts and S. Baroutian, A critical review on current urea removal technologies from water: An approach for pollution prevention and resource recovery, *Sep. Purif. Technol.*, 2023, 123652.
8 T. P. Brdarić, D. D. Aćimović, B. G. Savić Rosić, M. D. Simić, K. D. Stojanović, Z. M. Vranješ and D. Vasić Anićijević, Bibliometric Analysis of Nanostructured Anodes for Electro-Oxidative Wastewater Treatment, *Sustainability*, 2024, **16**(10), 3982.
9 L. Fan, Z. Tu and S. H. Chan, Recent development of hydrogen and fuel cell technologies: A review, *Energy Rep.*, 2021, **7**, 8421–8446.
10 Q. Xu, Z. Guo, L. Xia, Q. He, Z. Li, I. T. Bello, K. Zheng and M. Ni, A comprehensive review of solid oxide fuel cells operating on various promising alternative fuels, *Energy Convers. Manage.*, 2022, **253**, 115175.
11 R. Lan, S. Tao and J. T. Irvine, A direct urea fuel cell–power from fertiliser and waste, *Energy Environ. Sci.*, 2010, **3**(4), 438–441.
12 E. T. Sayed, T. Eisa, H. O. Mohamed, M. A. Abdelkareem, A. Allagui, H. Alawadhi and K.-J. Chae, Direct urea fuel cells: Challenges and opportunities, *J. Power Sources*, 2019, **417**, 159–175.
13 W. Xu, Z. Wu and S. Tao, Urea-based fuel cells and electrocatalysts for urea oxidation, *Energy Technol.*, 2016, **4**(11), 1329–1337.
14 D. Zhu, H. Zhang, J. Miao, F. Hu, L. Wang, Y. Tang, M. Qiao and C. Guo, Strategies for designing more efficient electrocatalysts towards the urea oxidation reaction, *J. Mater. Chem. A*, 2022, **10**(7), 3296–3313.
15 R. K. Singh and A. Schechter, Electrochemical investigation of urea oxidation reaction on β $Ni(OH)_2$ and $Ni/Ni(OH)_2$, *Electrochim. Acta*, 2018, **278**, 405–411.
16 L. Wang, Y. Zhu, Y. Wen, S. Li, C. Cui, F. Ni, Y. Liu, H. Lin, Y. Li and H. Peng, Regulating the local charge distribution of Ni active sites for the urea oxidation reaction, *Angew. Chem.*, 2021, **133**(19), 10671–10676.
17 G. Hopsort, D. P. Do Carmo, L. Latapie, K. Loubière, K. G. Serrano and T. Tzedakis, Progress toward a better understanding of the urea oxidation by electromediation of Ni(III)/Ni(II) system in alkaline media, *Electrochim. Acta*, 2023, **442**, 141898.
18 S. Wang, P. Xu, J. Tian, Z. Liu and L. Feng, Phase structure tuning of graphene supported Ni-NiO Nanoparticles for enhanced urea oxidation performance, *Electrochim. Acta*, 2021, **370**, 137755.
19 A. V. Munde, B. B. Mulik, P. P. Chavan and B. R. Sathe, Enhanced electrocatalytic activity towards urea oxidation on Ni nanoparticle decorated graphene oxide nanocomposite, *Electrochim. Acta*, 2020, **349**, 136386.
20 A. Abutaleb, Electrochemical oxidation of urea on NiCu alloy nanoparticles decorated carbon nanofibers, *Catalysts*, 2019, **9**(5), 397.
21 M. A. Abdelkareem, Y. Al Haj, M. Alajami, H. Alawadhi and N. A. Barakat, Ni-Cd carbon nanofibers as an effective catalyst for urea fuel cell, *J. Environ. Chem. Eng.*, 2018, **6**(1), 332–337.
22 Q. Zhang, F. M. Kazim, S. Ma, K. Qu, M. Li, Y. Wang, H. Hu, W. Cai and Z. Yang, Nitrogen dopants in nickel nanoparticles embedded carbon nanotubes promote overall urea oxidation, *Appl. Catal., B*, 2021, **280**, 119436.
23 I. M. Mohamed and C. Liu, Chemical design of novel electrospun CoNi/Cr nanoparticles encapsulated in C-nanofibers as highly efficient material for urea oxidation in alkaline media, *Appl. Surf. Sci.*, 2019, **475**, 532–541.

24 M. Yang, W. Ge, Z. Liu, Y. Lv, H. Wu and J. Zhang, Selectively etching manganese from nickel-manganese hydroxides *via* thiourea corrosion for urea electro-oxidation, *J. Alloys Compd.*, 2024, **981**, 173731.

25 H. Zhang, Y. Bai, X. Lu, L. Wang, Y. Zou, Y. Tang and D. Zhu, Ni-Doped MnO_2 Nanosheet Arrays for Efficient Urea Oxidation, *Inorg. Chem.*, 2023, **62**(12), 5023–5031.

26 M. A. Hefnawy, S. A. Fadlallah, R. M. El-Sherif and S. S. Medany, Synergistic effect of Cu-doped NiO for enhancing urea electrooxidation: Comparative electrochemical and DFT studies, *J. Alloys Compd.*, 2022, **896**, 162857.

27 W. Xu, H. Zhang, G. Li and Z. Wu, Nickel-cobalt bimetallic anode catalysts for direct urea fuel cell, *Sci. Rep.*, 2014, **4**(1), 5863.

28 S.-K. Geng, Y. Zheng, S.-Q. Li, H. Su, X. Zhao, J. Hu, H.-B. Shu, M. Jaroniec, P. Chen, Q.-H. Liu and S.-Z. Qiao, Nickel ferrocyanide as a high-performance urea oxidation electrocatalyst, *Nat. Energy*, 2021, **6**(9), 904–912.

29 H. Qiu and F. Zou, Nanoporous PtCo surface alloy architecture with enhanced properties for methanol electrooxidation, *ACS Appl. Mater. Interfaces*, 2012, **4**(3), 1404–1410.

30 J.-N. Zheng, L.-L. He, C. Chen, A.-J. Wang, K.-F. Ma and J.-J. Feng, One-pot synthesis of platinum3cobalt nanoflowers with enhanced oxygen reduction and methanol oxidation, *J. Power Sources*, 2014, **268**, 744–751.

31 C. Xu, Z. Tian and P. Shen, Oxide (CeO_2, NiO, Co_3O_4 and Mn_3O_4)-promoted Pd/C electrocatalysts for alcohol electrooxidation in alkaline media, *Electrochim. Acta*, 2008, **53**(5), 2610–2618.

32 M. A. Prathap, B. Satpati and R. Srivastava, Facile preparation of β-$Ni(OH)_2$-$NiCo_2O_4$ hybrid nanostructure and its application in the electro-catalytic oxidation of methanol, *Electrochim. Acta*, 2014, **130**, 368–380.

33 R. Armstrong and E. Charles, Some effects of cobalt hydroxide upon the electrochemical behaviour of nickel hydroxide electrodes, *J. Power Sources*, 1989, **25**(2), 89–97.

34 M. Yu, J. Chen, J. Liu, S. Li, Y. Ma, J. Zhang and J. An, Mesoporous $NiCo_2O_4$ nanoneedles grown on 3D graphene-nickel foam for supercapacitor and methanol electro-oxidation, *Electrochim. Acta*, 2015, **151**, 99–108.

35 W. Yan, D. Wang and G. G. Botte, Nickel and cobalt bimetallic hydroxide catalysts for urea electro-oxidation, *Electrochim. Acta*, 2012, **61**, 25–30.

36 N. A. M. Barakat, M. Motlak, B.-S. Kim, A. G. El-Deen, S. S. Al-Deyab and A. M. Hamza, Carbon nanofibers doped by Ni_xCo_{1-x} alloy nanoparticles as effective and stable non precious electrocatalyst for methanol oxidation in alkaline media, *J. Mol. Catal. A: Chem.*, 2014, **394**, 177–187.

37 N. A. M. Barakat, M. Motlak, A. A. Elzatahry, K. A. Khalil and E. A. M. Abdelghani, Ni_xCo_{1-x} alloy nanoparticle-doped carbon nanofibers as effective non-precious catalyst for ethanol oxidation, *Int. J. Hydrogen Energy*, 2014, **39**(1), 305–316.

38 W. Iqbal, A. Hameed, I. Tariq, S. S. A. Shah and M. A. Nadeem, Cobalt hydroxide supported nickel nanoparticles for an efficient electrocatalytic urea oxidation reaction, *Electrochim. Acta*, 2023, **467**, 143055.

39 Y. Liu, J. Guan, W. Chen, Y. Wu, S. Li, X. Du and M. Zhang, Nickel-cobalt derived nanowires/nanosheets as electrocatalyst for efficient H_2 generation *via* urea oxidation reaction, *J. Alloys Compd.*, 2022, **891**, 161790.

40 X.-H. Wang, Q.-L. Hong, Z.-N. Zhang, Z.-X. Ge, Q.-G. Zhai, Y.-C. Jiang, Y. Chen and S.-N. Li, Two-dimensional nickel–cobalt bimetallic hydroxides towards urea electrooxidation, *Appl. Surf. Sci.*, 2022, **604**, 154484.

41 M. M. Ismail, A. A. Farghali and A. G. El-Deen, Rational design of cobalt oxide nanocubes arrays on Ni foam as durable and robust electrocatalyst for urea electro-oxidation, *Beni-Suef Univ. J. Basic Appl. Sci.*, 2024, **13**(1), 123.

42 S. Yadav, A. Sharma Ghrera and A. Devi, Hierarchical grass-like $NiCo_2O_4$ nanowires grown on nickel foam as a binder-free supercapacitor electrode, *Mater. Today: Proc.*, 2023, **74**, 281–288.

43 H. Rong, T. Chen, R. Shi, Y. Zhang and Z. Wang, Hierarchical $NiCo_2O_4$@$NiCo_2S_4$ Nanocomposite on Ni Foam as an Electrode for Hybrid Supercapacitors, *ACS Omega*, 2018, **3**(5), 5634–5642.

44 K. Peng, N. Bhuvanendran, F. Qiao, G. Lei, S. Y. Lee and H. Su, Coupling NiMn-Layered Double Hydroxide Nanosheets with $NiCo_2S_4$ Arrays as a Heterostructure Catalyst to Accelerate the Urea Oxidation Reaction, *ACS Appl. Nano Mater.*, 2023, **6**(19), 18318–18327.

45 K. Peng, L. Liu, N. Bhuvanendran, F. Qiao, G. Lei, S. Y. Lee, Q. Xu and H. Su, Effective regulation on catalytic performance of nickel–iron–vanadium layered double hydroxide for urea oxidation *via* sulfur incorporation, *Mater. Adv.*, 2023, **4**(5), 1354–1362.

46 N. Wu, R. Guo, X. Zhang, N. Gao, X. Chi, D. Cao and T. Hu, Nickel/nickel oxide nanocrystal nitrogen-doped carbon composites as efficient electrocatalysts for urea oxidation, *J. Alloys Compd.*, 2021, **870**, 159408.

47 R. Shi, Y. Zhang and Z. Wang, Facile synthesis of a $ZnCo_2O_4$ electrocatalyst with three-dimensional architecture for methanol oxidation, *J. Alloys Compd.*, 2019, **810**, 151879.

48 J. Yin, H. U. Lee and J. Y. Park, An electrodeposited graphite oxide/cobalt hydroxide/chitosan ternary composite on nickel foam as a cathode material for hybrid supercapacitors, *RSC Adv.*, 2016, **6**(41), 34801–34808.

49 X. Hu, X. Tian, Y.-W. Lin and Z. Wang, Nickel foam and stainless steel mesh as electrocatalysts for hydrogen evolution reaction, oxygen evolution reaction and overall water splitting in alkaline media, *RSC Adv.*, 2019, **9**(54), 31563–31571.

50 B. Cao, C. Luo, J. Lao, H. Chen, R. Qi, H. Lin and H. Peng, Facile synthesis of 3d transition-metal-doped α-$Co(OH)_2$ nanomaterials in water–methanol mediated with ammonia for oxygen evolution reaction, *ACS Omega*, 2019, **4**(15), 16612–16618.

51 C. Xing, F. Musharavati, H. Li, E. Zalezhad, O. K. Hui, S. Bae and B.-Y. Cho, Synthesis, characterization, and properties of nickel–cobalt layered double hydroxide nanostructures, *RSC Adv.*, 2017, **7**(62), 38945–38950.

52 J. Yang, H. Liu, W. N. Martens and R. L. Frost, Synthesis and characterization of cobalt hydroxide, cobalt oxyhydroxide, and cobalt oxide nanodiscs, *J. Phys. Chem. C*, 2010, **114**(1), 111–119.

53 A. Kumar, S. K. Purkayastha, A. K. Guha, M. R. Das and S. Deka, Designing Nanoarchitecture of NiCu Dealloyed Nanoparticles on Hierarchical Co Nanosheets for Alkaline Overall Water Splitting at Low Cell Voltage, *ACS Catal.*, 2023, **13**(16), 10615–10626.

54 H.-Y. Wang, J.-T. Ren, L. Wang, M.-L. Sun, H.-M. Yang, X.-W. Lv and Z.-Y. Yuan, Synergistically enhanced activity and stability of bifunctional nickel phosphide/sulfide heterointerface electrodes for direct alkaline seawater electrolysis, *J. Energy Chem.*, 2022, **75**, 66–73.

55 H. Li, P. Liu, Y. Liang, J. Xiao and G. Yang, Amorphous cobalt hydroxide nanostructures and magnetism from green electrochemistry, *RSC Adv.*, 2013, **3**(48), 26412–26417.

56 Y. Yan, R. Wang, Q. Zheng, J. Zhong, W. Hao, S. Yan and Z. Zou, Nonredox trivalent nickel catalyzing nucleophilic electrooxidation of organics, *Nat. Commun.*, 2023, **14**(1), 7987.

57 B. Baruah, R. Biswas and P. Deb, Hybrid 2D-1D nanostructure of NiO composited with PEDOT:PSS and rGO: Bifunctional electrocatalyst towards methanol oxidation and oxygen evolution reaction, *Int. J. Energy Res.*, 2022, **46**(12), 16394–16415.

58 M. A. Abdelkareem, Y. Al Haj, M. Alajami, H. Alawadhi and N. A. M. Barakat, Ni-Cd carbon nanofibers as an effective catalyst for urea fuel cell, *J. Environ. Chem. Eng.*, 2018, **6**(1), 332–337.

59 T. Yuan, J. Yang, Y. Wang, H. Ding, X. Li, L. Liu and H. Yang, Anodic diffusion layer with graphene-carbon nanotubes composite material for passive direct methanol fuel cell, *Electrochim. Acta*, 2014, **147**, 265–270.

60 R. K. Mallick, S. B. Thombre, R. V. Motghare and R. R. Chillawar, Analysis of the clamping effects on the passive direct methanol fuel cell performance using electrochemical impedance spectroscopy, *Electrochim. Acta*, 2016, **215**, 150–161.

61 Q. Zhou, T.-T. Li, F. Guo and Y.-Q. Zheng, Construction of Hierarchically Structured CuO@CoP Anode for Efficient Oxygen Evolution Reaction, *ACS Sustain. Chem. Eng.*, 2018, **6**(9), 11303–11312.

62 W. Shi and J. Lian, Mesoporous $Cu(OH)_2$ nanowire arrays for urea electrooxidation in alkaline medium, *Mater. Chem. Phys.*, 2020, **242**, 122517.

63 A. Karmakar and S. Kundu, A concise perspective on the effect of interpreting the double layer capacitance data over the intrinsic evaluation parameters in oxygen evolution reaction, *Mater. Today Energy*, 2023, **33**, 101259.

64 K. Akbar, J. H. Jeon, M. Kim, J. Jeong, Y. Yi and S.-H. Chun, Bifunctional Electrodeposited 3D $NiCoSe_2$/Nickle Foam Electrocatalysts for Its Applications in Enhanced Oxygen Evolution Reaction and for Hydrazine Oxidation, *ACS Sustain. Chem. Eng.*, 2018, **6**(6), 7735–7742.

65 X. Zhu, X. Dou, J. Dai, X. An, Y. Guo, L. Zhang, S. Tao, J. Zhao, W. Chu and X. C. Zeng, Metallic nickel hydroxide nanosheets give superior electrocatalytic oxidation of urea for fuel cells, *Angew. Chem., Int. Ed.*, 2016, **55**(40), 12465–12469.

66 D. Zhu, C. Guo, J. Liu, L. Wang, Y. Du and S.-Z. Qiao, Two-dimensional metal–organic frameworks with high oxidation states for efficient electrocatalytic urea oxidation, *Chem. Commun.*, 2017, **53**(79), 10906–10909.

67 E. T. Sayed, A. H. Alami, M. A. Abdelkareem, T. Wilberforce, S. K. Kamarudin and A. G. Olabi, Real Direct Urea Fuel Fell Operation Using Standalone Ni-based Metal-Organic Framework Prepared by Ball Mill at Room Temperature, *Energy*, 2024, 132164.

68 T. Q. N. Tran, B. J. Park, W. H. Yun, T. N. Duong and H. H. Yoon, Metal–organic framework-derived Ni@C and NiO@C as anode catalysts for urea fuel cells, *Sci. Rep.*, 2020, **10**(1), 278.

69 Z. Wang, W. Liu, Y. Hu, M. Guan, L. Xu, H. Li, J. Bao and H. Li, Cr-doped CoFe layered double hydroxides: Highly efficient and robust bifunctional electrocatalyst for the oxidation of water and urea, *Appl. Catal., B*, 2020, **272**, 118959.

70 S. Feng, L. Yang, P. Deng, J. Wang, R. Xu, X. Liu, W. Wang, X. Tian and Z. Wu, Hierarchical self-supported $NiSe_2$/TiN@$Ni_{12}P_5$ on nickel foam for the urea oxidation reaction, *Int. J. Hydrogen Energy*, 2022, **47**(87), 36814–36822.

71 M. A. Abdelkareem, E. T. Sayed, H. O. Mohamed, M. Obaid, H. Rezk and K.-J. Chae, Nonprecious anodic catalysts for low-molecular-hydrocarbon fuel cells: Theoretical consideration and current progress, *Prog. Energy Combust. Sci.*, 2020, **77**, 100805.

72 X. Zhao, Y. Wang, Y. Zhang, S. Luo, H. Zhang and D. Y. Leung, Ni-Fe Layered Double Hydroxide Nanosheets Supported on Exfoliated Graphite for Efficient Urea Oxidation in Direct Urea Fuel Cells, *ChemSusChem*, 2022, **15**(7), e202102614.

73 Y. Tong, P. Chen, M. Zhang, T. Zhou, L. Zhang, W. Chu, C. Wu and Y. Xie, Oxygen vacancies confined in nickel molybdenum oxide porous nanosheets for promoted electrocatalytic urea oxidation, *ACS Catal.*, 2018, **8**(1), 1–7.